CMT Ceramics in Modern Technologies
TECHNA GROUP srl

A Novel Approach to Additive Manufacturing of Alkali-activated Materials: Laser-induced Slip Casting (LIS) of Lithium Aluminate/Silica Slurries

Petr Hlaváček[a], Gregor J.G. Gluth[a]*, Jörg Lüchtenborg[a], Patrick Sturm[a], Thomas Mühler[b], Hans-Carsten Kühne[a], Jens Günster[a]
[a]Bundesanstalt für Materialforschung und -prüfung (BAM), Berlin, Germany; [b]Technische Universität Clausthal, Institute of Non-Metallic Materials, Clausthal-Zellerfeld, Germany

Additive manufacturing of alkali-activated materials currently attracts a lot of attention, because of the possibility to produce customized high-performance elements for a range of applications, potentially being more resource-efficient than conventionally produced parts. Here, we describe a new additive manufacturing process for alkali-activated materials that is based on selective laser-heating of lithium aluminate/microsilica slurries. The new process-material combination allows to manufacture elements with complex geometries at high building rates and high accuracy. The process is versatile and transferrable to structures of sizes differing by orders of magnitude. The mechanical strength of the obtained materials was in the range of values reported for conventional metakaolin-based geopolymers, and superior to what has been hitherto reported for alkali-activated materials produced by additive manufacturing. This mechanical performance was obtained despite the fact that the degree of reaction of the lithium aluminate and the microsilica was low, suggesting that significant reactions took place only at the surface of the microsilica particles.

Keywords: Additive manufacturing; 3D printing; Laser-induced slip casting; Alkali-activated materials; Lithium aluminosilicates.

1. Introduction

Alkali-activated materials (AAMs) is the term commonly used to denote materials that are produced by the reaction of aluminosilicate precursors (such as metallurgical slags, metakaolin, coal fly ashes or volcanic glasses) with an alkaline solution (alkali hydroxide, alkali silicate, alkali carbonate etc.). The phase assemblage of AAMs is determined to a large extent by the amount of calcium in the system, with Ca-rich systems (e.g., based on blast furnace slag) generally leading to poorly crystalline calcium aluminosilicate hydrates as the major reaction products, and Ca-poor systems (e.g. based on metakaolin) leading to amorphous to semi-crystalline alkali aluminosilicate gels. These latter materials are often referred to as 'geopolymers', if all Al and Si in the structure is four-fold coordinated by oxygen, and the $(Al,Si)O_4$ tetrahedra form an amorphous three-dimensional aluminosilicate network [1]. Important applications of AAMs include binders for concretes and mortars in civil engineering and in waste stabilization (due to high mechanical strength and durability and the ability to fix various ions, respectively) [2-5], fire-proofing and refractory materials (due to a high resistance against high temperatures) [5-9] as well as precursors for ceramics [10-12]. Because of the wide range of applications, the mentioned beneficial engineering properties and the possibility to produce AAMs from industrial by-products such as slags and fly ashes, which can make them more cost-efficient and environmentally friendly than conventional cements and ceramics, AAMs have received a lot of attention from academia and industry in recent decades.

On the processing side, additive manufacturing holds great promise for the production of ceramics [13] as well as of concrete elements and even whole buildings [14, 15], offering more versatility and enabling production of elements that cannot be produced by a conventional route. In construction applications, additive manufacturing of elements can significantly lower or even remove framework cost, which is often in the range 35-60% of the total construction cost and can be even higher for complex geometries [15]. In the cases where AAMs are 'greener' than established materials [16], their combination with additive manufacturing technologies, which facilitates manufacture of exactly the geometries that are required, could be an additional contribution to more resource efficiency and, thus, more environmentally friendly construction and ceramic industries. Furthermore, properties like acid resistance [17, 18] and high-temperature resistance [6-9, 19, 20] make AAMs promising candidates for increasing the functionality of parts, besides the benefit of the freedom in design gained by the additive manufacturing processes.

This has driven research into additive manufacturing of AAMs by different research groups using various technologies. Indirect additive manufacturing, using poly(lactic acid) sacrificial templates, has been applied to metakaolin-based geopolymers [21]. Powder-based 3D printing has been used to produce parts from a slag-based AAM, with the compressive strength of the post-processed

* *Corresponding author*
E-mail address: gregor.gluth@bam.de

https://doi.org/10.29272/cmt.2018.0011
Received September 6, 2018; Received in revised form October 29, 2018; Accepted November 6, 2018

materials up to 16.5 MPa [22]. The most promising approach up to now seems to be direct ink writing (DIW) of metakaolin-based geopolymers, which allows to produce *inter alia* complex scaffolds with a tailored pore structure [23, 24]. Comparatively high mechanical strengths for AAMs produced by additive manufacturing have been reported by Panda et al. [25], who applied the DIW process to glass fiber-reinforced, alkali-activated mortars with hard coal fly ash/blast furnace slag blends as solid feedstock; the compressive strengths of the materials after 28 days of curing at room temperature were in the range ~20-25 MPa, and flexural strengths were ~2.5-7 MPa, depending on the fiber content and the direction of the load. However, DIW of AAMs remains a challenging approach due to the necessity to strictly control the rheological properties of the ink and its evolution with time [23], and, moreover, composites such as fiber-reinforced materials are difficult to produce, as high fiber loadings of the ink will tend to clog the nozzle through which the material is extruded [25].

Usually, sodium or potassium hydroxide or silicate solutions are employed for the production of AAMs, mainly for economic reasons. However, the use of other alkali ions can provide advantages for specific applications. Cesium silicate-activated materials have been studied as precursors for ceramics, considering that pollucite [$Cs_2(Al_2Si_4O_{12})\cdot nH_2O$] is one of the most refractory known silicates [10]. The use of lithium as the alkali ion to produce AAMs has been studied in detail previously only by O'Connor & MacKenzie [11]. It was found that the Li-activated AAMs were composed mainly of Li-zeolites of the framework types ABW, EDI (edingtonite-like), LTA (Linde type A-like) and/or FAU (faujasite-like), depending on the employed SiO_2/Al_2O_3 ratio and the synthesis route. On heating up to 1250 °C, the materials transformed to β-eucryptite or β-spodumene, which possess excellent resistance to thermal shock, due to their low thermal expansion coefficients; the authors thus proposed the Li-based AAMs as cost-efficient precursors for lithium aluminosilicate glass-ceramics. This proposal is similar to earlier work [26], in which lithium aluminosilicate gels, produced by the sol-gel route from lithium alumina sols and silica (TEOS, fumed silica or rice husk ash) were suggested as economic precursors for β-eucryptite/β-spodumene glass-ceramics. The feasibility of AM of lithium aluminosilicate glass-ceramics via 3D indirect printing and subsequent sintering of glass powders has been demonstrated by Zocca et al. [27].

In this contribution, we present a novel method for additive manufacturing of Li-activated AAMs that evolves from previous experience with laser-induced slip casting (LIS) of inert ceramic suspensions [28, 29], and the reactions of sodium aluminate/microsilica-based one-part AAMs [18, 30]. In this method, a lithium aluminate/microsilica slurry is deposited layer-wise, and selectively heated by laser radiation to induce hardening reactions of the material; subsequently, the produced element is further cured at slightly elevated temperature for 24 h. We report temperature evolution during the process, mechanical strengths as well as SEM and XRD data, and discuss ways to further improve the produced materials.

2. Materials and Methods

2.1. Starting materials

The starting materials for the slurries were lithium aluminate (Sigma-Aldrich, St. Louis, MO, USA), two microsilica powders, and quartz flour (Quarzmehl W 3, Quarzwerke GmbH, Frechen/plant Weferlingen, Germany).

The lithium aluminate was mainly composed of γ-$LiAlO_2$ (PDF # 00-038-1464), but in addition contained smaller amounts of $LiAl_5O_8$ (PDF # 00-038-1425) as well as minor quantities of $LiAl_2(OH)_7\cdot 2H_2O$ (PDF # 00-040-0710), corundum (α-Al_2O_3; PDF # 00-046-1212) and bayerite ($Al(OH)_3$; PDF # 00-020-0011) (cf. Fig. 5a).

Table 1. Chemical compositions of the starting materials.

Component	Lithium aluminate (wt%)	Microsilica RW (wt%)	Microsilica Q1 (wt%)	Quartz flour (wt%)
SiO_2	3.00	94.57	94.21	97.93
Al_2O_3	77.94	0.17	0.38	0.38
Fe_2O_3	0.01	0.04	0.05	0.05
TiO_2	< 0.02	0.01	0.03	0.03
CaO	< 0.01	1.15	0.49	0.04
MgO	< 0.02	0.23	0.25	< 0.01
Li_2O	21.77	-	-	-
Na_2O	-	0.14	0.55	0.15
K_2O	0.01	0.71	0.64	0.05
SO_3	< 0.02	0.21	0.56	0.02
P_2O_5	-	0.14	0.24	0.14
LOI[a]	1.65	1.84	1.88	0.57

[a] LOI: Loss on ignition; -: not determined

Two microsilica powders were employed; these are designated microsilica RW (SiO_2 'RW-Füller', RW silicium GmbH, Pocking, Germany) and microsilica Q1 (SiO_2 'RW-Füller Q1', RW silicium GmbH, Pocking, Germany). The two microsilicas were very similar in terms of chemical composition (Table 1) and phase composition: Both microsilicas were virtually fully amorphous, including only very minor amounts of silicon carbide (PDF # 00-049-1429), and silicon (PDF # 00-001-0787) or quartz (PDF # 00-046-1045) impurities (cf. Fig. 5). Both microsilicas consisted of spherical primary particles with diameters of about 50-300 nm, and they performed virtually identical in all experiments.

The quartz flour was virtually pure quartz (PDF # 00-046-1045); its nominal particle size range was 0-250 μm (manufacturer's data).

2.2. Mix-designs of the slurries

Slurries were produced by first blending dry lithium aluminate and microsilica in amounts to yield an overall SiO_2/Al_2O_3 molar ratio of 3.5. Subsequently, the dry blends were mixed with water at a water-to-solids ratio (w/s) of 0.50. Two microsilica powders – RW and Q1 – were used, but these were virtually identical in terms of composition and particle morphology (Section 2.1.). For the sake of completeness, however, a distinction between RW and Q1 will always be made in the sample designations: The materials produced from these slurries will be referred to below as MS_LiAl_RW (produced with microsilica RW) or MS_LiAl_Q1 (produced with microsilica Q1).

Additional slurries were produced by blending lithium aluminate/microsilica mixes (with SiO_2/Al_2O_3 = 3.5, as above) with an equal mass of quartz flour and subsequent mixing of the resulting powder with water at w/s = 0.50. The materials produced from these slurries will be referred to as MS_LiAl_3.5_[QF] (produced with microsilica RW) or MS_LiAl_Q1_[QF] (produced with microsilica Q1).

2.3. The LIS process

For manufacturing of parts, the slurries were subjected to laser-induced slip casting (LIS). The LIS process is an iteration of the deposition of a layer of slurry and subsequent local heating of

the desired geometry in this layer by a laser beam [28, 29]. The employed set-up consisted of a 100-W CO_2 laser system (λ = 10.6 µm; SC10, Rofin, Hamburg, Germany), equipped with a laser scanner (hurrySCAN, Scanlab AG, Munich, Germany) for inscription of the desired geometry, and a building platform that can be moved in height, i.e. z-direction. The building platform was connected to a linear drive to be stepwise lowered in a container filled with the slurry (Fig. 1).

The layer thickness, defined by the z-displacement of the building platform between two laser curing steps, was chosen as 960 µm. When the platform was lowered, the slurry overflowed the building platform and the already printed parts; the flow of the slurry was supported by a doctor blade to generate a constant layer thickness. In each layer, those regions that constitute the part to be produced, previously defined and stored as a sliced CAD file, were annealed by laser radiation (cf. Fig. 1). The laser power was set to 33 W; the spot size (diameter) of the focused beam on the surface of the slurry varied between 770 µm and 1100 µm, depending on the distance between the surface of the slurry and the laser source at the beginning of the experiment. The element was scanned with a speed of 2000 mm/s and a hatch distance (distance between two neighboring laser scanning paths) of 25 µm.

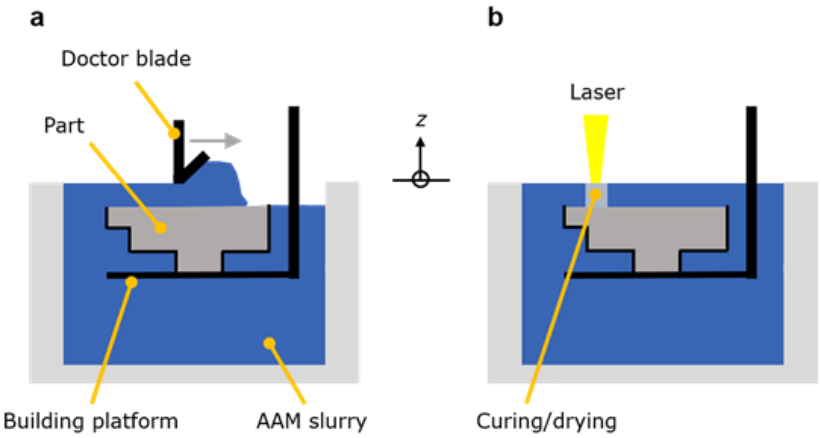

Figure 1. Schematic of the LIS set-up and process. In the deposition step (a), the slurry is overflowing the previously annealed part, aided by movement of a doctor blade. In the subsequent curing step (b), the slurry is locally annealed by laser radiation. After completion of the curing step, the building platform with the part is lowered (moved in negative z-direction) and the steps are repeated until the part is finished.

After finishing LIS of a part, it was removed from the container, rinsed with water, and allowed to dry in air for ~24 h. Subsequently, the part was sealed in a plastics bag and transferred to an oven, where it was additionally cured for 24 h at 80 °C.

For demonstration purposes, various miniaturized pipe system manifolds, up to approx. 100 mm × 100 mm × 70 mm in size were produced. In addition, beams with dimensions 10 mm × 10 mm × 60 mm or 18 mm × 18 mm × 96 mm were produced for mechanical testing. Pieces of the parts were ground with mortar and pestle (agate) for XRD analyses. Specimens for scanning electron microscopy (SEM) were cut with a water-cooled precision saw. Some of these specimens were subsequently embedded in epoxy resin under vacuum, cut, and the cross-sections ground and polished before SEM analyses.

During production of all parts, the temperature at the surface of the slurry was continuously monitored during the LIS process with a thermal imaging camera (A655sc, FLIR, Wilsonville, OR, USA). For one of the manifolds, the data was recorded for subsequent analysis.

2.4. Mechanical testing

Mechanical testing was performed on a static materials testing machine (Z010, Zwick/Roell, Ulm, Germany). Flexural strength was measured with the layers parallel to the external loads, i.e. without imposing shear stress between the layers. Compressive strength was measured perpendicular to the layers (denoted 'horizontal') as well as parallel to the layers (denoted 'vertical'). All mechanical properties reported are the mean of the results of at least two specimens.

2.5. Analytical methods

Scanning electron microscopy (SEM) was performed on a EVO MA10 instrument (Carl Zeiss, Jena, Germany), using the secondary electron (SE) detector to study the morphology of cut and polished surfaces.

X-ray diffraction (XRD) patterns of powdered specimens were recorded on an Ultima IV diffractometer (Rigaku, Tokyo, Japan) in Bragg-Brentano geometry under the following conditions: Cu Kα radiation (λ = 1.5419 Å), 40 kV, 40 mA; divergence slit: 0.5° axial, 10 mm in-plane; sampling interval = 0.02° 2θ; scan rate = 0.5° 2θ min^{-1}; scanning range: 5-65° 2θ; strip detector D/teX Ultra. Samples were rotated at a speed of 15 min^{-1} during the measurements.

3. Results

3.1. Temperature evolution during the LIS process

During the LIS process, the temperature at the surface of the slurry increased to up to ~100 °C at the locations where the laser radiation interacted with the slurry (Fig. 2). At these temperatures, the solubility of the microsilica is increased compared to room temperature [31], and the temperature increase will generally accelerate the kinetics of the dissolution of the starting materials and the precipitation of reaction products. In addition, evaporation of water and associated liquid transport in the slurry leads to movement of the solid particles in the slurry that tend to increase the packing density of the particles [29].

Temperatures slightly higher than 100 °C were recorded in cases when the laser heated parts of the surface repeatedly within a short time period (Fig. 2d), implying that drying was rather complete at the peak temperatures during this stage. However, it can be assumed that during fabrication of subsequent layers the surrounding solution is able to penetrate the porous green body at least partly [29], enabling resumption of the hardening reactions.

3.2. Example parts and mechanical strength

The novel LIS process allowed to produce parts with high accuracy, leading to a homogeneous appearance of their surfaces (Fig. 3). No significant sagging of overhangs and spanning elements could be observed by visual inspection.

To obtain a first indication whether the materials were properly cured and stable AAMs and not only bound by dried alkali silicate, their solubility in water was assessed by a simple immersion test, as has been done previously for AAMs produced by novel synthesis routes [32, 33]. Pieces of MS_LiAl_RW_[QF] and MS_LiAl_Q1 (each ~2-3 cm^3) were immersed in beakers with ~300 cm^3 tap water for 9 weeks (water filled up to ~300 cm^3 approx. weekly). This immersion did not lead to disintegration or any observable signs of deterioration or significant dissolution, indicating the presence of a stable, insoluble binder matrix. However, a slight yellowish coloring of the water in which MS_LiAl_Q1 was

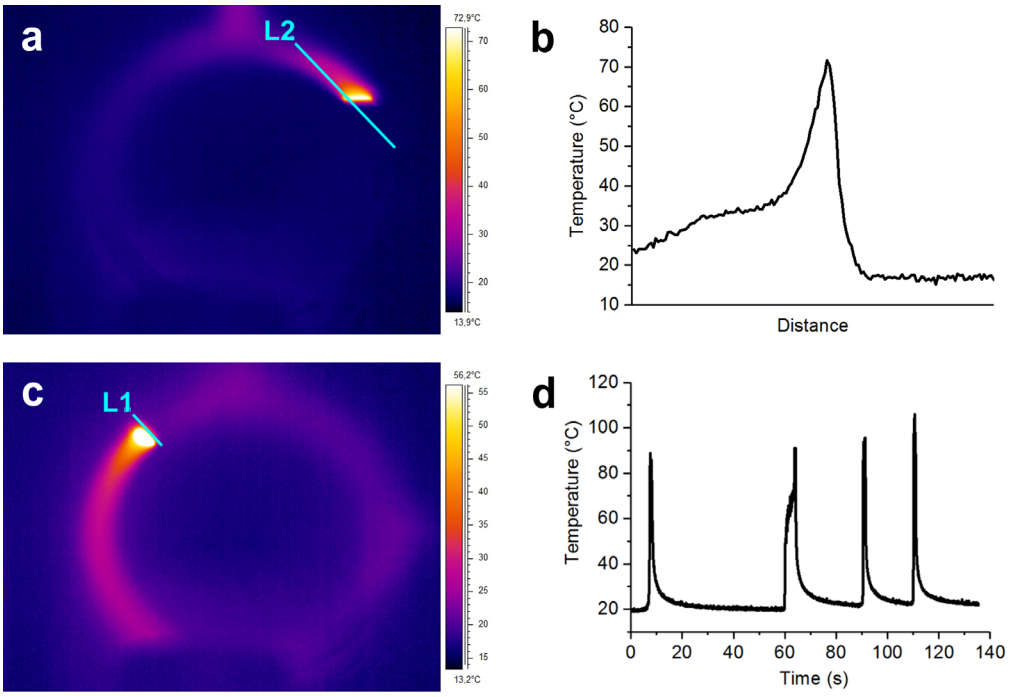

Figure 2. Thermal imaging during the production of a manifold with the LIS process. The outer diameter of the circular wall of the manifold is 10 cm (cf. Fig. 3). (a) snapshot showing line L2 with a length of ~4.7 cm; (b) temperature along line L2; (c) snapshot showing line L1; (d) evolution of the maximum temperature along line L1 vs. time.

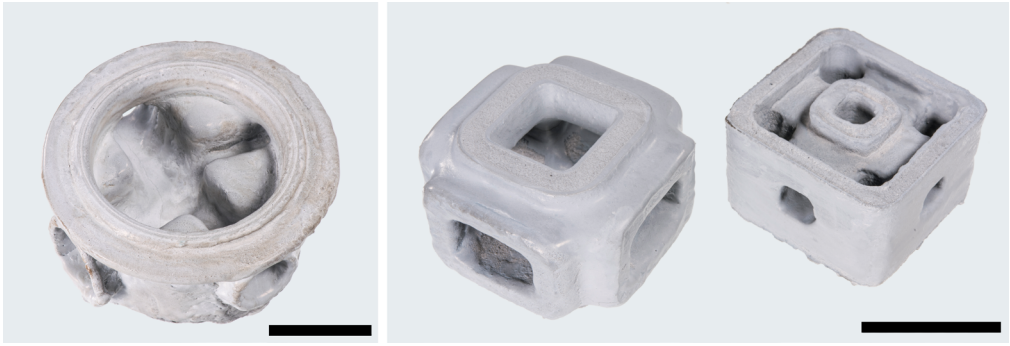

Figure 3. Manifolds produced from MS_LiAl_Q1_[QF]; scale bars are 40 mm.

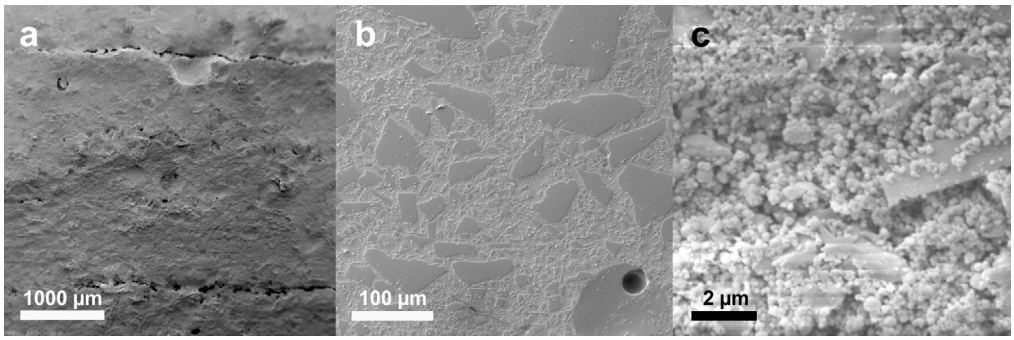

Figure 4. SEM micrographs of MS_LiAl_RW_[QF]. (a) cut surface, showing imperfect bond between some layers; (b) polished surface, showing quartz flour particles embedded in an apparently homogeneous matrix; (c) detail of cut surface, showing microsilica and quartz flour particles.

Table 2. Compressive and flexural strength of beam specimens (one standard deviation given after the plus/minus sign).

	Compressive strength: vertical (MPa)	Compressive strength: horizontal (MPa)	Flexural strength (MPa)
MS_LiAl_RW_[QF][a]	22.1 ± 1.3	-	11.6 ± 0.2
MS_LiAl_RW_[QF][b]	37.6 ± 4.4	49.3 ± 2.1	6.3 ± 1.9

[a] beam cross-section 10 mm × 10 mm; [b] beam cross-section 18 mm × 18 mm; -: not determined

immersed was observed, indicating release of minor or trace elements, possibly iron. The compressive and flexural strengths of MS_LiAl_RW_[QF] were up to ~50 MPa and ~12 MPa, respectively (Table 2). In the case where the compressive strength was measured perpendicular to the layers ('horizontal') as well as parallel to the layers ('vertical'), the strength perpendicular to the layers was higher. As the material contains quartz flour as a filler, comparison of these values should be made with particle-reinforced AAMs. Sá Ribeiro et al. [34] have reviewed the mechanical properties of conventionally produced, metakaolin-based geopolymers with particle or fiber reinforcement, and reported compressive strengths in the range 14-109 MPa, and three-point flexural strengths in the range 3.1-16.8 MPa for these materials. Thus, the strengths of MS_LiAl_RW_[QF] produced in the present study by LIS are well within the ranges of metakaolin-based geopolymers, i.e. AAMs produced by the conventional route.

3.3. SEM micrographs

SEM shows that the microstructure of the materials produced by LIS was inhomogeneous on different length scales. First, porous interfaces existed between some (but not all) of the layers that were defined by the stepwise lowering of the building platform (Fig. 4a). The irregular occurrence of these porous interfaces indicates that imperfect bonding between successive layers is not an inherent issue of the process, but instead probably depends on subtle variations of process parameters such as smoothness of the surface of the part before deposition of a new layer of slurry and/or viscosity of and heat transfer within the slurry during laser-induced heating. In any case, this issue warrants further optimization of the LIS process. Second, as expected, the angular quartz flour particles appeared as fillers in

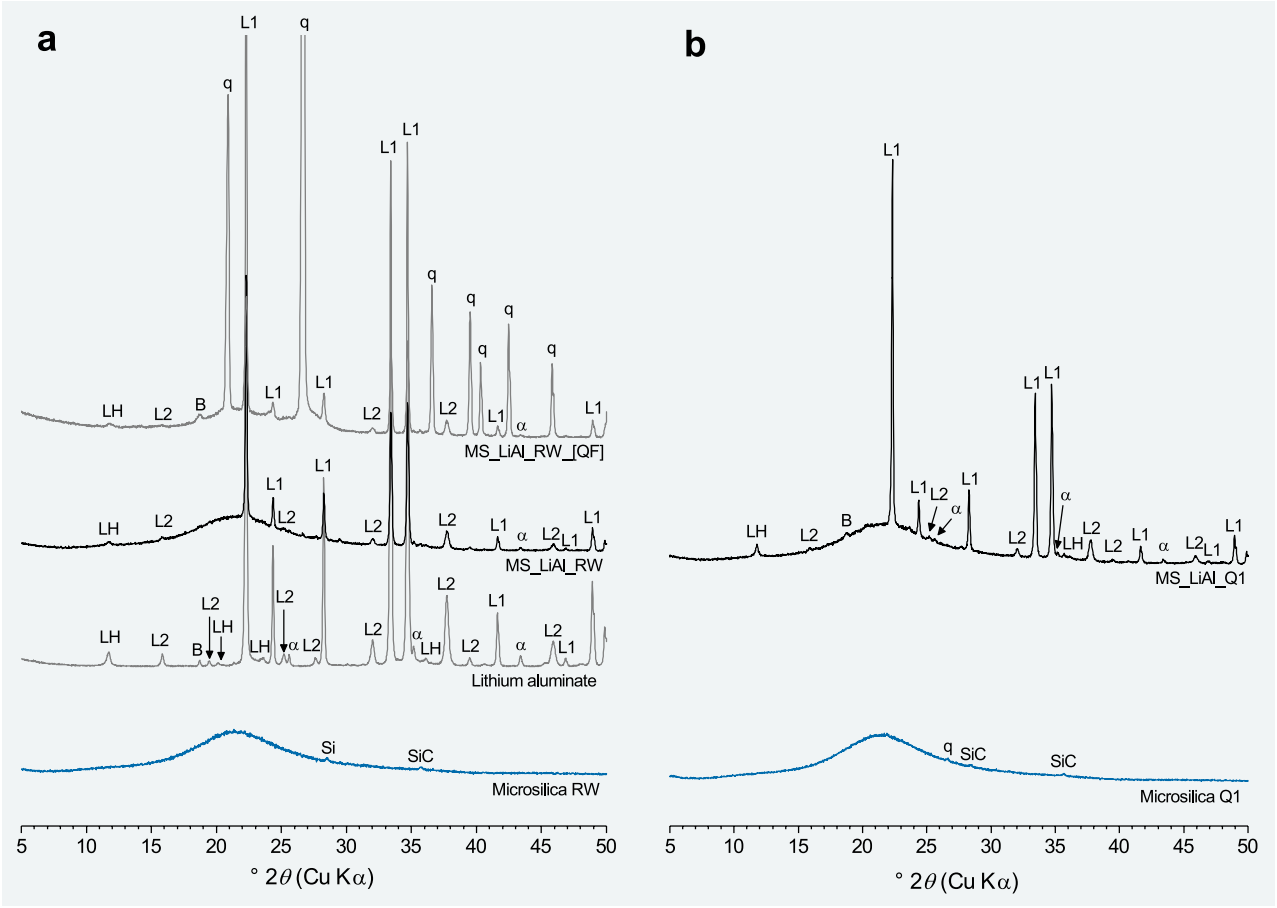

Figure 5. XRD patterns (Cu Kα radiation) of (a) MS_LiAl_RW_[QF] and MS_LiAl_RW, the lithium aluminate, and the microsilica RW; (b) MS_LiAl_Q1 and the microsilica Q1. Major reflections are labelled L1-γ-$LiAlO_2$; L2-$LiAl_5O_8$; LH-$LiAl_2(OH)_7{\cdot}2H_2O$; α-corundum; B-bayerite; q-quartz; Si-silicon; SiC-silicon carbide.

an apparently homogeneous binder matrix (Fig. 4b). However, the micrograph recorded at higher magnification (Fig. 4c) shows that, third, the binder matrix between the quartz particles consisted of spherical microsilica particles that were only partially dissolved, leaving significant interparticle porosity.

3.4. XRD analyses

X-ray diffractograms of the microsilicas, the lithium aluminate and the LIS-produced materials are shown in Fig. 5. The only significant difference between the LIS-produced materials with and without quartz flour – MS_LiAl_RW_[QF] and MS_LiAl_RW – is the presence of intense reflections of quartz in the diffractogram of the material with quartz flour, while the relative intensities of the reflections of the other compounds were not significantly altered. This indicates that the quartz flour acted as a filler without affecting the formation of crystalline phases (e.g., via heterogeneous nucleation) in the binder matrix.

Both microsilicas exhibited the typical, broad amorphous hump, centered at ~22° 2θ, in their diffractograms. This hump was present, nearly unaltered, in the XRD patterns of the LIS-produced materials too. This confirms that the microsilica had dissolved and reacted only to a very limited extent, in line with the SEM observations.

The reflections of all phases that were present in the starting lithium aluminate were observed in the diffractograms of the LIS-produced materials too, without significant changes of their relative intensities. Thus, as is the case with the microsilica, the results show that dissolution of the lithium aluminate occurred only to a limited extend during the LIS process and curing.

No crystalline phases other than the compounds already present in the starting materials were detected in the diffractograms of the LIS-produced materials, and the diffractograms do not indicate the formation of significant amounts of additional $LiAl_2(OH)_7{\cdot}2H_2O$ or bayerite during LIS and curing. However, minor formation of $LiAl_2(OH)_7{\cdot}2H_2O$ cannot be excluded based on the XRD results only.

4. Discussion and Conclusions

From the insolubility in water and the mechanical properties of the materials produced by the LIS process, it can be inferred that reaction products had formed during the LIS process, and these products bond the microsilica and lithium aluminate particles at their contact points to form stable parts. The thus obtained mechanical properties are comparable to conventionally produced AAMs. The inferred formation of reaction products means that, contrary to our earlier work on the LIS-process [28, 29], the solid particles in the slurry were slightly reactive, i.e. that the local laser heating did not induce the formation of a green body by purely physical means (drying), but that some dissolution and precipitation took place in the slurry where it was locally heated, i.e. chemical reactions led to formation the solid parts.

Lithium aluminosilicate solutions would be expected to precipitate the zeolites Li-EDI and/or Li-ABW at elevated temperatures (40-100 °C) [11, 35]. Despite synthesis temperatures in the same range, crystallization of zeolites or significant amounts of other crystalline products did not occur during the LIS process of lithium aluminate/silica slurries in the present study. This can probably be attributed to the water-deficiency of the system, analogous to what is generally observed with Na- or K-activated systems, in which zeolite crystallization would be expected at high water/solid ratios, but does not, or only to a limited degree, occur at the

water contents that are applied to produce AAMs [36].

Barrer and White [37] reported the formation of an 'uncrystallized' gel with the composition $LiO_2{\cdot}Al_2O_3{\cdot}3SiO_2$ and a high sorption capacity (i.e. high specific surface area) by drying a lithium aluminosilicate solution at 120 °C. In more recent work [26], lithium aluminosilicate gels were produced by the sol-gel route from lithium alumina sols and silica materials, including fumed silica, involving temperatures of 80 °C. A parsimonious explanation for the observations made in the present study would be that an amorphous lithium aluminosilicate gel, analogous to those observed in the two latter studies, has formed during the LIS process. Spectroscopic studies are required to determine whether the Si and the Al in the product(s) occur indeed in a single phase, or instead in separate phases; what the 'best' crystalline analog for the reaction product(s) would be; and what the main reason for the beneficial properties of the binder phase(s) is. However, due to the low amounts of reaction products in the material, it will be challenging to derive conclusive data on these issues, even with advanced methods; thus, a more promising approach may be to design suitable model systems and study these.

In addition, future work should investigate the use of other activators as well as the effect of varying the relative amounts of the feedstocks and filler(s) in the slurry. Optimization of the process/material combination may further increase the mechanical strength of the produced parts by minimizing the extent of inhomogeneities such as the porous interfaces observed between some of the layers. Introduction of fibers and/or reinforcing particles other than quartz flour can be expected to additionally contribute to improved mechanical properties; the laser-based LIS process lends itself easier to this option than AM technologies that require extrusion of a paste.

References

[1] K.J.D. MacKenzie, What are these things called geopolymers? A physicochemical perspective, Ceram. Trans. 153 (2003) 175-186.

[2] D.M. Roy, Alkali-activated cements: opportunities and challenges, Cem. Concr. Res. 29 (1999) 249-254.

[3] H. Xu, J.L. Provis, J.S.J. van Deventer, P.V. Krivenko, Characterization of aged slag concretes, ACI Mater. J. 105 (2008) 131-139.

[4] J.L. Provis, D.G. Brice, A. Buchwald, P. Duxson, E. Kavalerova, P.V. Krivenko, C. Shi, J.S.J. van Deventer, J.A.L.M. Wiercx, Demonstration projects and applications in building and civil infrastructure, in: J.L. Provis, J.S.J. van Deventer (Eds.), Alkali Activated Materials: State-of-the-Art Report, RILEM TC 224-AAM, Springer, Dordrecht, 2014, pp. 309-338.

[5] S.A. Bernal, P.V. Krivenko, J.L. Provis, F. Puertas, W.D.A. Rickard, C. Shi, A. van Riessen, Other potential applications for alkali-activated materials, in: J.L. Provis, J.S.J. van Deventer (Eds.), Alkali Activated Materials: State-of-the-Art Report, RILEM TC 224-AAM, Springer, Dordrecht, 2014, pp. 339-380.

[6] K. Sakkas, D. Panias, P.P. Nomikos, A.I. Sofianos, Potassium based geopolymer for passive fire protection of concrete tunnel linings, Tunn. Undergr. Space Technol. 43 (2014) 148-156.

[7] P. Hlaváček, V. Šmilauer, F. Škvara, L. Kopecký, R. Šulc, Inorganic foams made from alkali-activated fly ash: mechanical, chemical and physical properties, J. Eur. Ceram. Soc. 35 (2015) 703-709.

[8] M.-B. Watolla, G.J.G. Gluth, P. Sturm, W.D.A. Rickard, S. Krüger, B. Schartel, Intumescent geopolymer-bound coatings for fire protection of steel, J. Ceram. Sci. Technol. 8 (2017) 351-364.

[9] D.C. Comrie, W.M. Kriven, Composite cold ceramic geopolymer in a refractory application, Ceram. Trans. 153 (2003) 211-225.

[10] J.L. Bell, P.E. Driemeyer, W.M. Kriven, Formation of ceramics from metakaolin-based geopolymers: Part I - Cs-based geopolymer, J. Am. Ceram. Soc. 92 (2009) 1-8.

[11] S.J. O'Connor, K.J.D. MacKenzie, Synthesis, characterisation and thermal behaviour of lithium aluminosilicate inorganic polymers, J. Mater. Sci. 45 (2010) 3707-3713.

[12] C. Kuenzel, L.M. Grover, L. Vandeperre, A.R. Boccaccini, C.R. Cheeseman, Production of nepheline/quartz ceramics from geopolymer mortars, J. Eur. Ceram. Soc. 33 (2013) 251-258.

[13] A. Zocca, P. Colombo, C.M. Gomes, J. Günster, Additive manufacturing of ceramics: issues, potentialities, and opportunities, J. Am. Ceram. Soc. 98 (2015) 1983-2001.

[14] T. Wangler, E. Lloret, L. Reiter, N. Hack, F. Gramazio, M. Kohler, M. Bernhard, B. Dillenburger, J. Buchli, N. Roussel, R. Flatt, Digital concrete: opportunities and challenges, RILEM Tech. Lett. 1 (2016) 67-75.

[15] M. Bechthold, J.C. Weaver, Materials science and architecture, Nat. Rev. Mater. 2 (2017) 17082.

[16] P. Duxson, J.L. Provis, G.C. Lukey, J.S.J. van Deventer, The role of inorganic polymer technology in the development of 'green concrete', Cem. Concr. Res. 37 (2007) 1590-1597.

[17] A. Fernandez-Jimenez, I. García-Lodeiro, A. Palomo, Durability of alkali-activated fly ash cementitious materials, J. Mater. Sci. 42 (2007) 3055-3065.

[18] P. Sturm, G.J.G. Gluth, C. Jäger, H.J.H. Brouwers, H.-C. Kühne, Sulfuric acid resistance of one-part alkali-activated mortars, Cem. Concr. Res. 109 (2018) 54-63.

[19] W.D.A. Rickard, G.J.G. Gluth, K. Pistol, In-situ thermo-mechanical testing of fly ash geopolymer concretes made with quartz and expanded clay aggregates, Cem. Concr. Res. 80 (2016) 33-43.

[20] L. Carabba, S. Manzi, E. Rambaldi, G. Ridolfi, M.C. Bignozzi, High-temperature behaviour of alkali-activated composites based on fly ash and recycled refractory particles, J. Ceram. Sci. Technol. 8 (2017) 377-388.

[21] G. Franchin, P. Colombo, Porous geopolymer components through inverse replica of 3D printed sacrificial templates, J. Ceram. Sci. Technol. 6 (2015) 105-112.

[22] M. Xia, J. Sanjayan, Method of formulating geopolymer for 3D printing for construction applications, Mater. Des. 110 (2016) 382-390.

[23] G. Franchin, P. Scanferla, L. Zeffiro, H. Elsayed, A. Baliello, G. Giacomello, M. Pasetto, P. Colombo, Direct ink writing of geopolymeric inks, J. Eur. Ceram. Soc. 37 (2017) 2481-2489.

[24] A. Rincón Romero, H. Elsayed, E. Bernardo, Highly porous mullite ceramics from engineered alkali activated suspensions, J. Am. Ceram. Soc. 101 (2018) 1036-1041.

[25] B. Panda, S.C. Paul, M.J. Tan, Anisotropic mechanical performance of 3D printed fiber reinforced sustainable construction material, Mater. Lett. 209 (2017) 146-149.

[26] M. Chatterjee, M.K. Naskar, Sol–gel synthesis of lithium aluminum silicate powders: the effect of silica source, Ceram. Int. 32 (2006) 623-632.

[27] A. Zocca, C.M. Gomes, E. Bernardo, R. Müller, J. Günster, P. Colombo, LAS glass-ceramic scaffolds by three-dimensional printing, J. Eur. Ceram. Soc. 33 (2013) 1525-1533.

[28] T. Mühler, J. Heinrich, J. Günster, Verfahren zur laser-induzierten additiven Erzeugung eines Grünkörpers mittels Schlickerguss [Method for the additive laser-induced production of a main part by means of slip casting], German Patent DE102015110360 (A1) (2016).

[29] J. Lüchtenborg, T. Mühler, F. Léonard, J. Günster, Laser-induced slip casting (LIS) - a new additive manufacturing process for dense ceramics demonstrated with Si_3N_4, J. Ceram. Sci. Technol. 8 (2017) 531-540.

[30] P. Sturm, S. Greiser, G.J.G. Gluth, C. Jäger, H.J.H. Brouwers,

Degree of reaction and phase content of silica-based one-part geopolymers investigated using chemical and NMR spectroscopic methods, J. Mater. Sci. 50 (2015) 6768-6778.
[31] G.B. Alexander, W.M. Heston, R.K. Iler, The solubility of amorphous silica in water, J. Phys. Chem. 58 (1954) 453-455.
[32] D.R.M. Brew, K.J.D. MacKenzie, Geopolymer synthesis using silica fume and sodium aluminate, J. Mater. Sci. 42 (2007) 3990-3993.
[33] G.J.G. Gluth, C. Lehmann, K. Rübner, H.-C. Kühne, Geopolymerization of a silica residue from waste treatment of chlorosilane production, Mater. Struct. 46 (2013) 1291-1298.
[34] R.A. Sá Ribeiro, M.G. Sá Ribeiro, W.M. Kriven, A review of particle- and fiber-reinforced metakaolin-based geopolymer composites. J. Ceram. Sci. Technol. 8 (2017) 307-322.
[35] T. Matsumoto, T. Miyazaki, Y. Goto, Synthesis and characterization of Li-type EDI zeolite, J. Eur. Ceram. Soc. 26 (2006) 455-458.
[36] P. Duxson, A. Fernández-Jiménez, J.L. Provis, G.C. Lukey, A. Palomo, J.S.J. van Deventer, Geopolymer technology: the current state of the art, J. Mater. Sci. 42 (2007) 2917-2933.
[37] R.M. Barrer, E.A.D. White, The hydrothermal chemistry of silicates. Part I. Synthetic lithium aluminosilicates, J. Chem. Soc. (1951) 1267-1278.